CONSTRUCTION PROGRESS OF THE RHIC ELECTRON LENSES*

W. Fischer†, Z. Altinbas, M. Anerella, E. Beebe, M. Blaskiewicz, D. Bruno, W.C. Dawson, D.M. Gassner, X. Gu, R.C. Gupta, K. Hamdi, J. Hock, L.T. Hoff, A.K. Jain, R. Lambiase, Y. Luo, M. Mapes, A. Marone, T.A. Miller, M. Minty, C. Montag, M. Okamura, A.I. Pikin, S.R. Plate, D. Raparia, Y. Tan, C. Theisen, P. Thieberger, J. Tuozzolo, P. Wanderer, S.M. White, W. Zhang
Brookhaven National Laboratory, Upton, New York, USA

Abstract

In polarized proton operation the RHIC performance is limited by the head-on beam-beam effect. To overcome this limitation two electron lenses are under construction. We give an overview of the construction progress. Guns, collectors and the warm electron beam transport solenoids with their power supplies have been constructed. The superconducting solenoids that guide the electron beam during the interaction with the proton beam are near completion. A test stand has been set up to verify the performance of the gun, collector and some of the instrumentation. The infrastructure is being prepared for installation, and simulations continue to optimize the performance.

INTRODUCTION

In the RHIC polarized proton operation the luminosity is limited by the head-on beam-beam effect, which will be mitigated by an electron lens in each ring. This, together with a new polarized proton source that is under construction [1], will allow for higher bunch intensities, and RHIC is being prepared for the higher total intensity [2].

The defocusing beam-beam kick that a proton receives from the other beam in one of the two interactions will be reversed by the electron lens in the same turn. For optimum compensation the electron beam size and current must be matched to the proton beam, and the phase advance between the beam-beam interaction and electron lens must be a multiple of π. In the most recent RHIC run [3] new power supplies were successfully tested that adjust the vertical phase advance, while phase shifters for the horizontal plane will be installed this year. The tolerable deviations from the optimum compensation parameters were studied extensively in simulations [4, 5].

The layout of the electron lenses is given in Refs. [6, 7] and the main parameters for the proton and electron beams are given in Tab. 1. An electron lens consists of an electron gun, an electron transport channel with 3 warm solenoids (GS1, GS2, GSB) and a steering dipole in both transverse planes (GSX/GSY), a superconducting solenoid in which the electron beam interacts with the proton beam, another electron transport channel mirror-symmetric to the previous one (CSB, CSX/CSY, CS2, CS1) and an electron collector. Most of the electron beam diagnostics are near the collector. The RHIC electron lens design built on the experiences gained with the Tevatron electron lenses [9] and the BNL Electron Beam Ion Source (EBIS) [10].

* Work supported by Brookhaven Science Associates, LLC under Contract No. DE-AC02-98CH10886 with the U.S. Department of Energy.

† Wolfram.Fischer@bnl.gov

Table 1: Reference Case for RHIC Beam-Beam and Beam-Lens Interactions [6, 7]

quantity	unit	value
proton beam parameters		
total energy E_p	GeV	250
bunch intensity N_p	10^{11}	2.5
$\beta^*_{x,y}$ at IP6, IP8 (p-p)	m	0.5
$\beta^*_{x,y}$ at IP10 (p-e)	m	10.0
rms emittance ϵ_n, initial	mm mrad	2.5
rms beam size at IP6, IP8 σ^*_p	μm	70
rms beam size at IP10 σ^*_p	μm	310
rms bunch length σ_s	m	0.25
rms momentum spread $\delta p/p$	10^{-3}	0.30
hourglass factor F, initial	...	0.88
beam-beam parameter ξ/IP	...	0.013
electron lens parameters		
distance of center from IP	m	2.0
effective length L_e	m	2.1
kinetic energy E_e	keV	7.8
electron line density n_e	10^{11}m^{-1}	1.0
electrons in lens N_{e1}	10^{11}	2.1
electrons encountered N_{e2}	10^{11}	2.5
current I_e	A	0.85

GUN AND COLLECTOR

The gun (Fig. 1) provides an electron beam with parameters in Tab. 1. The current density in the center must reach 10 A/cm^2 to satisfy these requirements taking into account the Gaussian transverse profile and the available magnetic compression from the gun to the superconducting solenoid. The gun has 3 operating modes: (i) DC for continuous compensation; (ii) 100 Hz for electron beam positioning with BPMs – the electron current rises between the last 2 RHIC bunches and falls in the abort gap; (iii) 78 kHz for single-bunch compensation – rise and fall time as in the 100 Hz mode. Both guns and the power supplies allowing for the 3 operating modes have been built. LaB_6 and CeIr cathodes were manufactured at BINP in Novosibirsk [11].

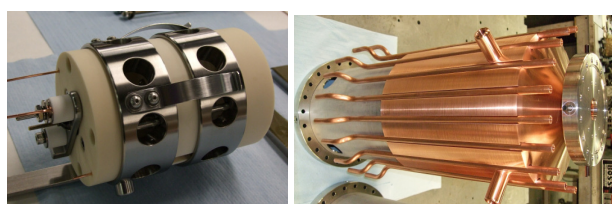

Figure 1: Gun (left), collector (right) during construction.

The collector spreads the electrons on the inside of a cylindrical surface that is water-cooled at the outside (Fig. 1). Simulations give a power density of 10 W/cm^2 for a 10 A electron beam, decelerated to 4 keV. The collector can

ISBN 978-3-95450-115-1

absorb up to 5 times this power density. Both collectors are completed and the collector power supplies are under construction.

WARM MAGNETS AND PS

The warm solenoid and steering magnets transport the electron beam from the gun to the superconducting solenoid and from the end of the solenoid to the collector. The main design considerations were a minimum field of 0.3 T for the electron transport at all locations, the field quality, and the available power and cooling power in the installation area [7, 8]. The three types GS1, GS2, GSB on the gun side (identical to CS1, CS2, CSB on the collector side) have a pancake design with currents of nominally 700-1200 A, and power consumption of 25 to 58 kW. Completed GS1, GS2, CS1, and CS2 magnets are shown in Fig. 2. The power supplies for the solenoids (one each for GS1 and CS1, GS2 and CS2, and GSB and CSB) were received and are being tested. The GSX/Y and CSX/Y steering magnets and their power supplies are under construction.

Figure 2: Completed GS1, GS2, CS1 and CS2 magnets.

SUPERCONDUCTING MAGNETS

A superconducting 6 T solenoid guides and stabilizes the low energy electron beam during the interaction with the proton beam, and allows for magnetic compression of the electron beam size to the proton beam size. The magnet has additional fringe field solenoids at the ends to facilitate the electron transport into and out of the solenoid. To maintain good field quality with large fringe fields and variable main field anti-fringe solenoids are added. The cryostat also contains 5 short horizontal and 5 short vertical dipole correctors to straighten the solenoid field lines, and a long horizontal and vertical dipole corrector to position the electron beam. Design details are given in [12].

Both solenoids, the 4 fringe and 4 anti-fringe solenoids, and all of the corrector magnets are wound. Fig. 3 shows the winding of the first solenoid. The first cold mass is completed and was installed in a vertical test Dewar. The second cold mass is near completion. The main solenoid in the first cold mass reached 5.56 T after 5 training quenches (Tab. 2), when a current to ground was detected. A decision was made not to use the first of the 11 double layers. This will lower the maximum field but may result in a magnet that does not need any training.

Table 2: Training history to date for the superconducting solenoid of the first cold mass. Design current and field are 440 A and 6 T respectively.

quench no	current [A]	field [T]	location
1	340	4.64	layer 1
2	366	5.00	layer 1
3	380	5.18	layer 1
4	389	5.30	layer 1
5	408	5.56	layer 1

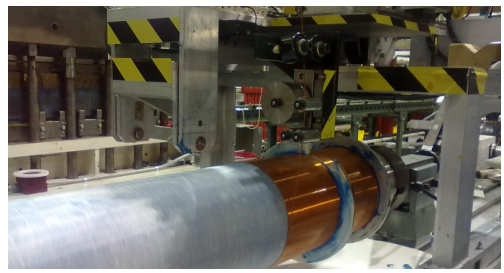

Figure 3: Superconducting solenoid during winding. The two visible end support plates are needed to contain the large axial forces [12].

With proton rms beam sizes of 310 μm in the electron lenses, a deviation of the solenoid field lines from straight lines of no more than 50 μm is targeted. A needle-and-mirror system has been constructed that can be used in the RHIC tunnel to both measure the straightness of the field lines, and verify the correction with the integrated short dipole correctors. The needle-and-mirror measurement system is being cross-checked with a vibrating wire system [13, 14] using the spare superconducting solenoid of the BNL EBIS.

INSTRUMENTATION

For the proton beam existing diagnostics will be used, including beam current and loss monitors, and beam transfer function (BTF) measurements. The electron beam instrumentation items and statuses are (i) beam position monitors (designed); (ii) halo monitors (manufactured for 1 lens); (iii) current monitor (completed for 1); (iv) drift tubes (designed); (v) collector temperature sensor (completed for 1); (vi) YAG screen profile monitor (completed for 1); (vii) pin hole detector (completed for 1).

The halo detector, YAG screen, and pin hole detector are all mounted in the same instrument holder, which has been manufactured (Fig. 4) and installed on the test bench. The drift tubes are used to extract the generated ions, which, in the DC operating mode would otherwise be trapped [15]. Major considerations in the design of the BPMs and drift tubes are the wake fields generated by the proton beam and the heating of the cables.

Previously it was planned to monitor the overlap of the electron and proton beams with the generated

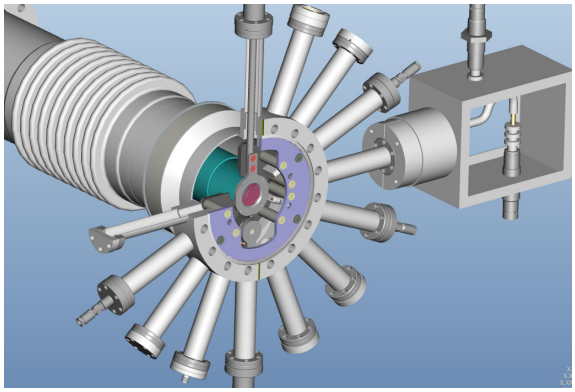

Figure 4: Instrument holder in front of the collector. Visible are the halo detector, YAG screen (inserted), and pin hole detector (retracted).

bremsstrahlung. The process that creates bremsstrahlung also creates back-scattered electrons, which can be observed in the vicinity of the electron beam as they travel along the magnetic field lines. This turned out to be easier than the extraction of the photons from the interaction region. A monitor was designed that detects the back-scattered electrons near the gun, where they penetrate a thin window and hit an electron detector (Fig. 5, [16]).

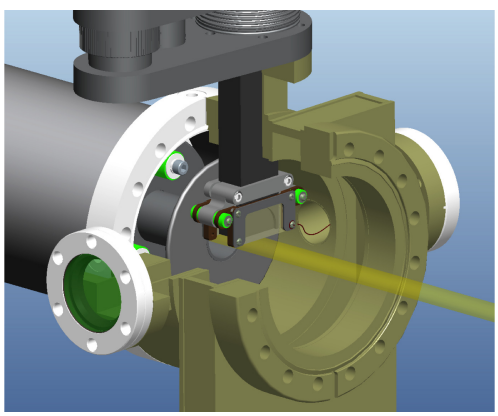

Figure 5: Detector for back-scattered electrons near the gun, to monitor the overlap of the electron and proton beams [16].

TEST BENCH

The test bench (Fig. 6) uses the location and the superconducting solenoid of the BNL EBIS test stand [17]. Of the RHIC electron lenses the following components are installed: a gun and collector, a GS1 solenoid with power supply, a movable pin hole detector, a movable YAG screen with camera, and an electron halo detector [18].

The goals of the test bench work are (i) measurement of the gun perveance; (ii) verification of the transverse Gaussian electron beam profile; (iii) demonstration of gun operation in all modes, i.e. 100 Hz, 78 kHz and DC; (iv) observation of the collector vacuum pressure and temperature with the highest possible load; (v) commissioning of the pin hole and YAG screen detectors; (vi) prototyping of the electron lens machine protection system; (vii) test of software controls and applications. The test bench work is in progress, more details are given in [19].

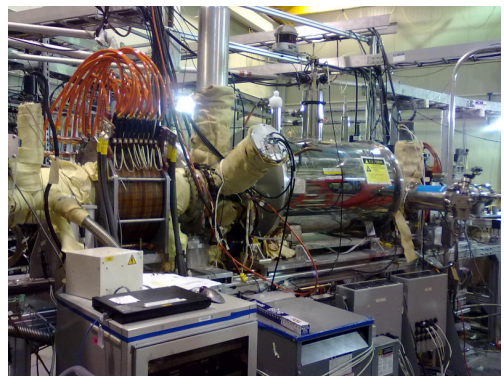

Figure 6: RHIC electron lens test bench. The electron beam travels from left to right, GS1 visible.

SUMMARY

The main components of the RHIC electron lenses are nearing completion. A test bench is set up to verify the gun and collector performance, and test a subset of the instrumentation. The infrastructure in RHIC is being prepared for installation in the summer of 2012.

ACKNOWLEDGMENTS

We are thankful for discussion and support to the personnel of the BNL Collider-Accelerator Department and Superconducting Magnet Division, Fermilab personnel working the Tevatron electron lenses, and others; in particular J. Alessi, M. Brennan, A. Fedotov, G. Ganetis, G. Kuznezov, K. Mirabella, A. Pendzick, T. Roser, L. Snydstrup, V. Shiltsev, G. Stancari, A. Valishev, and F. Zimmermann.

REFERENCES

[1] A. Zelenski, PAC'11 presentation.
[2] C. Montag et al., WEPPR021, these proceedings.
[3] V. Schoefer et al., MOPPC024, these proceedings.
[4] Y. Luo et al., PRSTAB, to be published.
[5] S. White, W. Fischer, and Y. Luo, MOPPC025, these proceedings.
[6] W. Fischer et al., IPAC'10, pp. 513 (2010).
[7] W. Fischer et al., PAC'11, pp. 2223-2225 (2011)
[8] X. Gu et al., NIM A 637, pp. 190-199 (2011).
[9] V. Shiltsev et al., PRSTAB 11, 103501 (2008).
[10] J. Alessi et al., PAC'11, pp. 1966-1968 (2011).
[11] G. Kuznezov, (2011).
[12] R. Gupta et al., PAC'11, pp. 1130-1132 (2011).
[13] A. Jain et al., IWAA08, TU010 (2008).
[14] A. Jain, presentation at IMMW17 (2011).
[15] X. Gu et al., THPPR032, these proceedings.
[16] P. Thieberger et al., BIW12, Newport News, VA (2012).
[17] E.N. Beebe et al., Journal of Physics: Conference Series 2 (2004) 164-173.
[18] D. Gassner et al., DIPAC2011, MOPD04 (2011).
[19] X. Gu et al., WEPPD084, these proceedings.

ISBN 978-3-95450-115-1